

Article

Investigation into the Gaseous SO₂ Attack on Sandstone in the Yungang Grottoes

Yue Zhang ^{1,2}, Cheng Cao ¹, Houmeng Du ^{1,2}, Jizhong Huang ^{1,*}, Xiuwei Guo ^{1,2}, Qingyang Luo ^{1,3} and Jianguang Ren ⁴

¹ Institute for the Conservation of Cultural Heritage, School of Cultural Heritage and Information Management, Shanghai University, Shanghai 200444, China

² School of Mechanics and Engineering Science, Shanghai University, Shanghai 200444, China

³ School of Materials Science and Engineering, Shanghai University, Shanghai 200444, China

⁴ Heritage Monitoring Center, Yungang Academy, Datong 037007, China

* Correspondence: hjizhong@163.com

Abstract: The Yungang Grottoes, with over 1500 years of history, have been subjected to air pollution since the last century. Field investigations have indicated that acid gases, particularly sulfur dioxide (SO₂), have accumulated on the surface of the sculptures and caused various types of decay that reduce their artistic value. To shed new light on the gas–stone interaction process, artificially accelerated weathering was performed on local sandstone in the laboratory. In a specially developed test device, fresh specimens were exposed to gaseous SO₂ under different relative humidity and temperature conditions. The physical, mineralogical, and chemical changes of Yungang sandstone were evaluated conjointly using destructive and non-destructive methods. The results show that after weathering, the luminosity of all specimens changed, with a slight alteration in hue toward yellow. The weight increased to various degrees during the aging cycles, which depended on both the accumulation of matter and the detachment of particles. Higher relative humidity and cyclic temperature fluctuations favored the dissolution of carbonates and the hydrolysis of feldspar in sandstone. The concentration of ions, especially dissolved Ca²⁺ and SO₄²⁻, increased considerably over time in the near-surface region of the specimens. A trace of newly formed gypsum was detected in some specimens at the end of the test. Knowing the synergistic impact of different climatic variables will make it possible to identify the mechanisms of the deterioration of sandstone in complex environments.

Keywords: Yungang Grottoes; sandstone deterioration; sulfur dioxide; climatic chamber; accelerated weathering; gypsum formation



Citation: Zhang, Y.; Cao, C.; Du, H.; Huang, J.; Guo, X.; Luo, Q.; Ren, J. Investigation into the Gaseous SO₂ Attack on Sandstone in the Yungang Grottoes. *Minerals* **2023**, *13*, 123.

<https://doi.org/10.3390/min13010123>

Academic Editors: Eduardo Molina, Giuseppe Cultrone and Salvador Domínguez

Received: 5 December 2022

Revised: 10 January 2023

Accepted: 11 January 2023

Published: 13 January 2023



Copyright: © 2023 by the authors. Licensee MDPI, Basel, Switzerland. This article is an open access article distributed under the terms and conditions of the Creative Commons Attribution (CC BY) license (<https://creativecommons.org/licenses/by/4.0/>).

1. Introduction

The aesthetic and mechanical characteristics of historical monuments and cultural heritage sites built of natural stones keep changing over time at different rates, depending on the natural and anthropogenic conditions they are exposed to. Their long-term performance is determined by interactions among various physical, chemical, and biological factors in different weathering processes. As a consequence of human activities, such as rapid industrial evolution and ever-growing social and economic life, air quality has become worse over the past few centuries. The negative influence of pollutants (atmospheric gases and airborne particulate matter) on stone structures, which has increased greatly on a global scale, has become a central concern for conservation professionals. Pollution-related surface deterioration manifests in various forms, such as patina-like depositions, soiling, and crusts from a few millimeters to centimeters thick. In particular, crust morphology changes, with colors ranging from white and gray to black, and with layers of laminar, framboidal, and cauliflower shapes [1–6]. This leads to the extensive destruction of stone

surfaces and, in the case of decorated surfaces, to the loss of ornamental details and thus reduced aesthetic value.

Sulfur dioxide (SO₂), one of the important causes of stone decay, mainly originates from the combustion of fossil fuels. This aggressive gas-phase air pollutant can be transferred to stone surfaces through dry and wet deposition processes [7]. When in contact with moisture, SO₂ can easily dissolve to form an acidic solution, which then triggers the chemical corrosion of rock-forming minerals. Due to the high sensitivity and reactivity to acidic environments, the sulfation process of calcareous stones, including limestone, marble, and travertine, has been a hot topic of research, with dozens of papers being published. To understand the kinetics of weathering, accelerated aging tests have been conducted on stones under laboratory conditions, and the progressive variations of physical, compositional, and microstructural characteristics have been analyzed [5,8–13]. In recent years, some attention has also been paid to SO₂-attacking stones with a relatively low content of calcium, such as granite, tuff, andesite, and trachyte, providing relevant information for assessing the type, rate, and degree of overall decay [4,12,14,15].

Sandstone, which is abundantly supplied and easily quarried, has been a lithotype commonly adopted for historical buildings and heritage sites worldwide. As a multiphase solid with a variety of mineral constituents cemented by fine binders, it forms a clastic texture characterized by different-sized grains, high porosity, and complex inner defects. Carbonates, which are included in sandstone as fragments, cement, or clays, are also susceptible to acid attack [16–18]. Gaseous pollutants can enter the material easily through its open pore network and interact with the components. Some researchers have investigated the sulfation of sandstone in simulated atmospheres considering various influencing factors, including the mineralogical composition (or, more precisely, the component of the binder matrix), the types and concentrations of polluting elements (gas and particles), the climatic conditions (temperature, air humidity, spray, and runoff), and so on [19–24]. Typically, stone samples were subjected to laboratory tests following two main protocols: acid solution immersion or acid atmosphere exposure. In one study, calcareous sandstones were immersed in aqueous H₂SO₄ solution with different pH values and the weight loss of the samples was measured periodically [25]. Using the Lausanne Atmospheric Simulation Chamber, Ausset et al. [26] simulated urban pollution on naked, soot-covered, and fly ash-covered sandstone samples for 12 months and compared the deposition velocity and penetration depth of SO₂ into the samples. Dewanckele et al. [27] explored the change of pore structure in a historical calcareous sandstone exposed to airborne SO₂ under wet surface conditions in Belgium. Using high-resolution X-ray computed tomography (CT), the weathering processes of the samples, such as dissolution, micro-crack initiation, and pore infilling, were clearly visualized. Additionally, variations in porosity, interconnectivity, and pore dimensions were quantified as a function of time.

As a major component of stone heritage sites in China, many grottoes can be found across the country, reflecting the evolutionary history of Buddhist art. More than 80% of them were actually dug in sandstone, sometimes with thin layers of mudstone and shale [28,29]. The natural weathering of these sites has been investigated for decades, but there are currently few studies on the contribution of air pollutants (especially SO₂) to the decaying of local materials [30–33]. In addition, the deterioration of heritage sandstone is usually not attributed to the effects of a specific single factor, but rather to the consequences of several factors under a multi-field coupled condition. Many decay processes interfere with each other, leading to eventual alteration patterns that are complex and dynamic. Yet, relevant information about the synergistic effects of other climatic variables on gaseous SO₂ attack is often neglected.

In light of these considerations, the purpose of this study was to gain a better understanding of the weathering characteristics, processes, and mechanisms of sandstone grottoes that remained unclear. The Yungang Grottoes, one of the most significant grotto heritage sites in China, were specifically selected. First, a field survey investigating common weathering features was conducted, including analyses of various weathering products

and the main deteriorating agents. Then, for further insight into the role of SO₂ in local sandstone weathering, accelerated aging tests were carried out in a specially-made climatic chamber under controlled environmental conditions. The influence of relative humidity (RH) and temperature were studied by precisely setting different target values. Changes in sandstone properties due to atmosphere–material interaction were assessed with the help of destructive and non-destructive methods. The test included visual inspection and mass weighing. The chemical and mineralogical compositions of fresh and weathered specimens were also compared using X-ray diffraction (XRD), X-ray fluorescence (XRF), and ion chromatography (IC). Finally, the deterioration mechanisms of Yungang sandstone were evaluated in detail to reveal the importance of each factor when acting in combination.

2. Field Investigation

2.1. Environmental Settings

The Yungang Grottoes, dating back to the Northern Wei Dynasty in the middle of the fifth century AD, are located in the north of Shanxi Province, about 16 km from Datong City. Overlooking a river valley, 45 major caves extend for 1 km from east to west at the southern foot of Wuzhou Mountain. Among them, 14 large caves over 10 m in height formed deep into the cliff. More than 50,000 carvings have remained on the walls and ceilings, impressing visitors with their rich content, magnificent appearance, exquisite workmanship, and universal value. As a well-known World Heritage Site and a National Key Cultural Relics Protection Unit, the Yungang Grottoes contain specific Chinese characteristics that are attributed to Buddhist cave art, which had a significant impact on the later cultures of China and East Asia.

Located in northern China, Datong City has a temperate continental semi-arid monsoon climate with four distinct seasons. Generally, it is characterized by warm and rainy summers and cold and dry winters, while spring and autumn are relatively cool. The average annual precipitation in Datong is between 400 and 500 mm, most of which concentrates in the summer. Variations in daily average values of air temperature and RH monitored at the Yungang Grottoes in 2017 are illustrated in Figure 1. During that 1-year period, the outdoor air temperature varied from -21.9 to 30.3 °C, with RH ranging from 11.1% to 96.9%. Clearly, the indoor air temperature and RH fluctuated in smaller ranges. For instance, the maximum and minimum air temperatures inside Cave 9 were -9.9 °C in January and 21.3 °C in July, while the RH was in the range of 32.9%–86.0%.

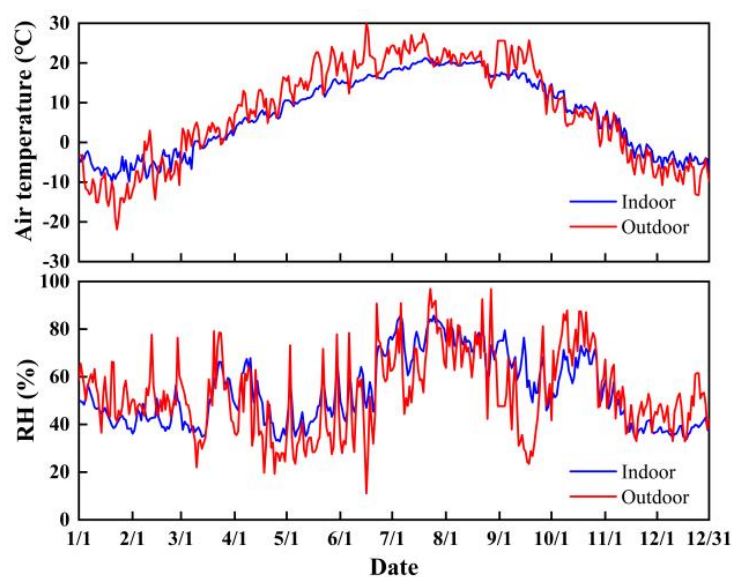


Figure 1. Average daily variations of indoor (Cave 9) and outdoor air temperature and RH in the Yungang Grottoes during 2017.

Datong is situated in the middle of one of China’s largest coal mining districts. As an industrial city, it suffers from very high levels of air pollution. Previously, a series of field monitoring experiments were conducted at the Yungang Grottoes to measure the concentrations of airborne particulate matter, both coarse and fine, as well as pollutant gases [34–36]. The major sources of gaseous SO₂ include the production of coal and its daily use, such as domestic heating and vehicle exhaust. Due to local environmental renovation projects over the past decades, an obvious decreasing trend of SO₂ pollution has been recorded [37]. The temporal distribution of SO₂ gas throughout the year has been uneven (Figure 2). As listed in Table 1, from 1991 to 2011, the maximum and minimum SO₂ concentrations are found in the winter (December to February) and summer (June to August), respectively. The annual mean SO₂ concentration dropped substantially from 0.767 (1991) to 0.363 mg/m³ (2001) and more recently to 0.059 mg/m³ (2011). The concentration in the winter was nearly double that of the annual mean, suggesting more consumption of fossil fuels at this time of year. The latest data (2021) show that SO₂ concentration became extremely low and the annual mean value was only 0.008 mg/m³.

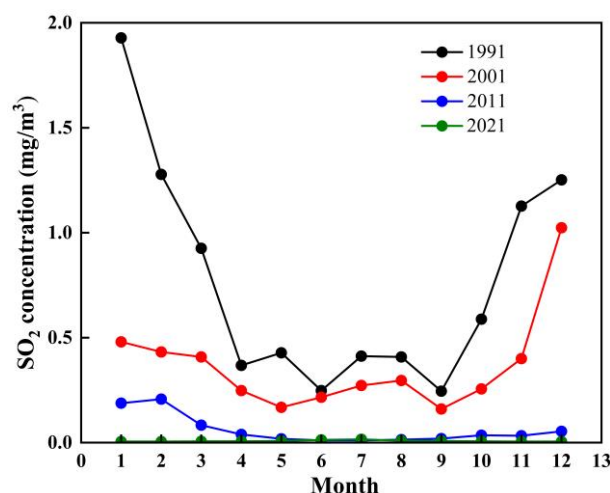


Figure 2. Average monthly variation of SO₂ concentration in the Yungang Grottoes.

Table 1. Seasonal variations of SO₂ concentration in the Yungang Grottoes.

Time	SO ₂ Concentration (mg/m ³)			
	1991	2001	2011	2021
Spring	0.574	0.275	0.047	0.007
Summer	0.356	0.261	0.012	0.013
Autumn	0.653	0.272	0.029	0.006
Winter	1.486	0.645	0.151	0.005
Annual mean	0.767	0.363	0.059	0.008

2.2. Characterization of Weathering Features

Weathering features can be divided into two categories: erosional and depositional. Erosional weathering removes material from stone by, for example, dissolution, exfoliation, flaking, scaling, or sanding; depositional weathering adds material to the stone’s surface by, e.g., efflorescence, encrustation, or biocolonization. Figure 3 presents some typical weathering features in the Yungang Grottoes, such as particulate deposition, surface discoloration, and salt efflorescence. Crusts are commonly observed on the outermost sandstone layers as well, showing variations in color, morphology, and thickness. These encrustations can eventually be detached from the substrate due to the dissolution of natural cementing materials beneath the crust. Alternatively, detachment can be also induced by actions behind the crust, such as ice and salt crystallization, hydration expansion, mechanical impact, thermal stress, and so on. This can lead to subsequent decay phenomena, from

the surface parallel formation (contour scaling, multiple flaking, etc.), to nondirectional manifestations (crumbling, granular disintegration, etc.). The newly exposed stone surface, located directly beneath the crust, is usually more porous and vulnerable to further weathering. Such erosive processes may not have an impact on the stability of structures, but will significantly affect the surface characteristics, especially for carved and painted elements of stone sculptures. This means catastrophic destruction and rapid loss of ornamental details and artistic information.

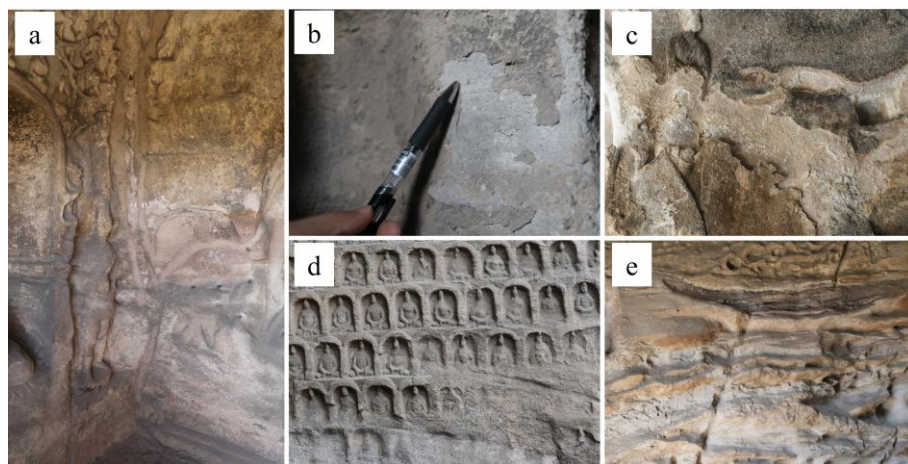


Figure 3. Typical weathering features in the Yungang Grottoes: (a) particulates deposition, surface discoloration, and salt efflorescence; (b) scaling of thin white crusts; (c) scaling of thick black crusts; (d) granular disintegration and surface recession; and (e) strip cutting.

Samples from various products of weathering were collected in the Yungang Grottoes for further identification. Considering the compromise between representativeness and restriction of sampling, different locations were selected based on the macroscopic evidence observed in the field, including disintegration, deposits, and crusts. As shown in Table 2, nine weathering products were sampled from four caves, which exhibited obvious distinctions in color, particle size, surface roughness, degree of cementation, pore structure, etc. The size of each sampling area was about 20 mm × 20 mm. The powder was gently removed using a mini brush, while the flakes (thinner than 2 mm) and blocks were carefully taken using tweezers from the sandstone surface. Fresh sandstone was also obtained at a hill nearby from the outcrops of contemporaneous strata extending horizontally to the grottoes. To avoid possible heterogeneity induced by natural weathering, blocks at a depth greater than 20 cm from the external surface were extracted and characterized for reference.

To analyze the chemical components, sandstone samples were characterized using a portable XRF. The weathering products had a significantly higher sulfur content (2.0%–6.3%) than the fresh sample (0.2%), implying an external source (Figure 4a). XRD patterns indicated that quartz was the dominant mineral in Yungang sandstone, together with K-feldspar, kaolinite, and a trace of calcite (Figure 4b). Compared to the fresh sample, there were obviously fewer carbonates in the weathering products. An additional constituent, gypsum, was also detected, especially in the blocky weathering products. This can be attributed to the fact that most caves at this site were built with entrances directly open to the outdoors, allowing gaseous pollutants, such as SO₂, to deposit on the sculptures without restriction. When moisture was present, a series of chemical reactions then occurred between the gas and mineral constituents in the sandstone, promoting the growth of newly formed products.

Clearly, despite the improvement in air quality in the Yungang Grottoes in recent years, sandstone deterioration due to exposure to atmospheric pollutants, particularly SO₂ gas, has occurred. At the same time, sculptures in the caves are constantly subjected to varying RH and air temperatures. Considering this scenario, exploratory experiments

were performed to reveal sandstone deterioration induced by gaseous SO₂ in the context of synergy with other environmental factors, as described in the following section.

Table 2. Details of sampling in the Yungang Grottoes.

No.	Weathering Products	Sampling Site	Macroscopic View	Microscopic View
1	Powdery	Eastern wall of Cave 4		
2		Northern wall of Cave 9		
3		Northern wall of Cave 12		
4	Flaky	Northern façade of the central pillar of Cave 4		
5		Northern wall of Cave 5		
6		Northwest corner of Cave 5		
7	Blocky	Eastern wall of Cave 4		
8		Eastern façade of the central pillar of Cave 4		
9		Northern wall of Cave 12		

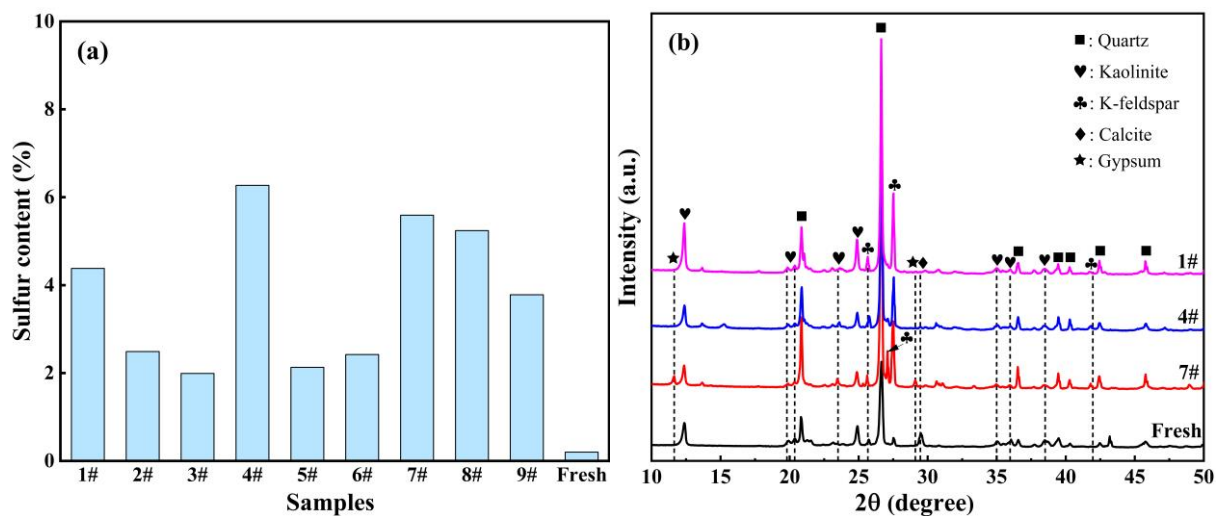


Figure 4. Chemical analysis of sandstone samples in the Yungang Grottoes: (a) sulfur content and (b) mineralogical composition.

3. Laboratory Experiments

3.1. Material

The Yungang Grottoes lie in the northwestern limb of the Jinhuaogong Syncline. The outcrop of sedimentary strata in this area is dominated by the Middle Jurassic Yungang Formation, a lens body of medium- to coarse-grained quartz sandstone interlayered with mudstone and sandy mudstone, covered by two layers of quaternary sediments. The sandstone contains mainly quartz, feldspar, calcite, and clay minerals such as kaolinite. The grain size varies in a wide range (from about 90 to 2000 μm), while the roundness changes from sub-rounded to sub-angular [29]. The texture can be characterized as grain-supported with pores filled by clay matrix and carbonate cement (Figure 5).

After cutting large blocks of fresh Yungang sandstone into 5 cm \times 5 cm \times 5 cm cubes, all specimens were oven-dried to constant mass at 105 $^{\circ}\text{C}$ and cooled to room temperature in a desiccator. For the sake of representativeness, cubes with similar P-wave velocities were screened out for further experiments. In total, 38 fresh specimens were selected, based on which the basic physical properties were determined; this number was considered sufficient due to the small dispersion of testing results (Table 3).

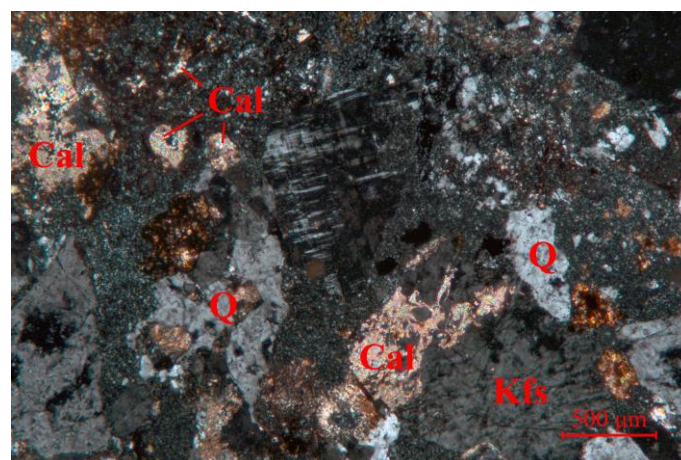


Figure 5. Photomicrograph of the texture of fresh Yungang sandstone (Q = quartz, Cal = calcite, and Kfs = K-feldspar).

Table 3. Basic physical properties of fresh Yungang sandstone.

Number of Specimens	Dry Density (g/cm ³)	Porosity (%)	Forced Water Absorption (mass, %)	P-Wave Velocity (m/s)	Hardness (HL)
38	2.37 ± 0.02	8.24 ± 0.17	3.64 ± 0.07	2587 ± 113	586 ± 29

3.2. Device

With the specific intention to investigate the impact of various environmental factors on sandstone, a test device was developed at the Institute for the Conservation of Cultural Heritage, Shanghai University (Figure 6). The main part of the weathering chamber has a space with an overall size of 0.4 m × 0.5 m × 0.5 m to accommodate specimens. The chamber is equipped with an LED light source inside and mid-hollow double-layer tempered glass windows on the top and sides for real-time monitoring of experiments.

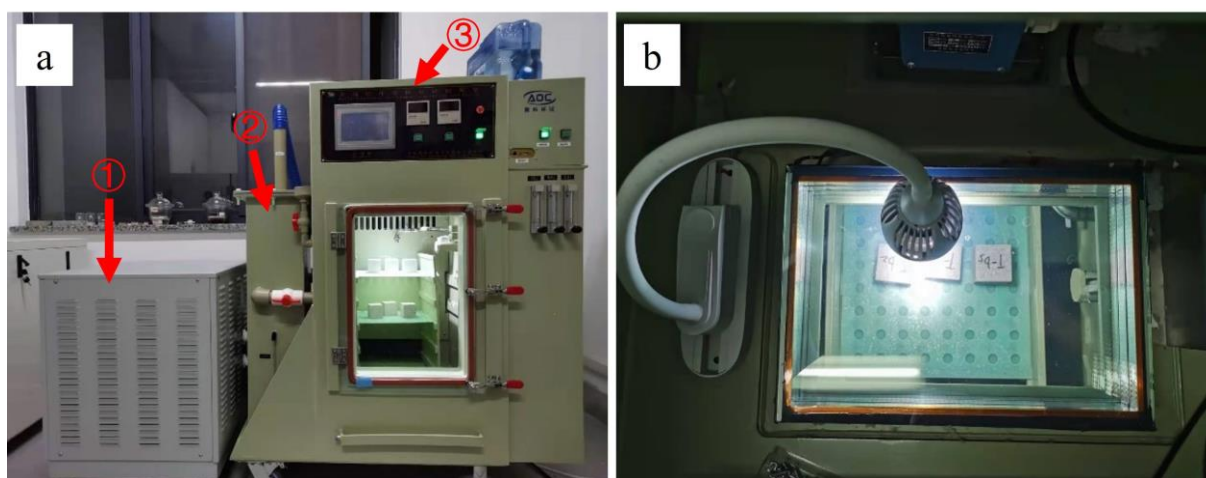


Figure 6. Pictures of test device: (a) side view and (b) top view. The main components include ① a refrigeration and dehumidification unit, ② an exhaust gas post-treatment system, and ③ a weathering chamber.

A programmable logic controller (PLC), to which actuators and sensors are connected, was adopted for the electrical system of the test device and operated by an advanced touch screen. The weathering chamber permits regulation of the inner temperature from 10 to 50 °C ($\pm 1\%$) and relative humidity from 40 to 90% ($\pm 5\%$). There is a rotating turret with an auxiliary spray nozzle centrally placed at the top inside the chamber with a maximum spray rate of 3 L/min, allowing the simulation of rainfall with varying intensities. Gaseous species (SO_2 , NO_2 , or CO_2) of high purity and certified quality are provided to the chamber from liquid gas cylinders via PTFE tubing. The gas injection rate is automatically monitored and adjusted by flow meters and time controllers installed at the inlet, while the gas concentration can be regulated within the limits of 10–300 ppm. To minimize the environmental impact of the polluting gases, an exhaust gas post-treatment system is also connected to the chamber, which is an alkali (aqueous solution of NaOH) impregnated filter with active carbon.

3.3. Methods

Artificially accelerated weathering tests were conducted to assess the effects of SO_2 , relative humidity, and temperature on sandstone degradation. The conditions under which the specimens were exposed are given in Table 4. The SO_2 concentration chosen in this study was 50 ppm ($=140 \text{ mg/m}^3$), which at first sight may appear to be above realistic values measured in the field. In fact, the deterioration process induced by polluted gas attacks is naturally very slow. For practical reasons, chamber studies are usually performed under extreme conditions in order to obtain reasonable results in a limited time. In addition,

the airflow (wind velocity) in outdoor environments is typically greater than what is practically possible in laboratory experiments. Thus, for compensation, the corresponding concentrations of pollutants in the lab have to be one or two orders of magnitude higher than those in the air [7]. Experiments with control groups were carried out under the exact same relative humidity and temperature conditions but without SO₂ gas. In each group, 6 duplicate specimens were evaluated.

Table 4. Environmental parameters of artificially accelerated weathering tests.

Specimens		SO ₂ Concentration (ppm)	RH (%)	Temperature (°C)	Testing Cycles
Testing group	RH40/T25	50	40	25	30
	RH80/T25		80	25	
	RH80/T15-45		80	15–45	
Control group	RH40/T25	0	40	25	
	RH80/T25		80	25	
	RH80/T15-45		80	15–45	

The detailed experimental procedure was as follows. First, desiccated cubes of fresh Yungang sandstone were placed on a rack inside the weathering chamber with all environmental parameters set to the target values for 12 h. The specimens were not coated, i.e., all sides were exposed to the atmosphere. In the case of RH80/T15-45, the inner temperature varied instead of being constant during this period. More specifically, the chamber was heated from 15 to 45 °C at a rate of 1 °C/min and then maintained for 1 h. Immediately after that, the temperature was decreased to 15 °C again over 30 min and remained there for 1 h. The chamber was programmed to automatically carry out this temperature fluctuation 4 times within 12 h. Second, the specimens were continuously stored enclosed in the weathering chamber for another 12 h at constant RH (preset value) and temperature (25 °C) but with no SO₂ gas. At this point, one weathering cycle of 24 h was completed.

In total, 30 cycles were carried out. For weathering assessment, changes in the physical and chemical properties of Yungang sandstone were determined periodically during this process. Surface characteristics and color changes were studied using a digital microscope (Hirox RH-2000, Tokyo, Japan) with a 40× binocular magnifier and a spectrophotometer (3nh YS3010, Shenzhen, China), respectively. Elemental composition was assessed with a handheld XRF analyzer (Thermo Scientific Niton XL3t GOLDD+, Waltham, MA, USA). The device is capable of detecting and measuring up to 30 elements, from magnesium to uranium, and provides real-time data instantly. Due to the use of much less energy, portable XRF has limited ability to penetrate deeply into a material. In general, the measurement only allows sampling at the outer surface of the specimen on the micron scale. For these three properties, the measurement was always performed at the same place on the top surface of the specimen in a non-destructive way. Weight changes were monitored by an electronic balance (PWN523ZH/E, OHAUS, Pine Brook, MN, USA) with an accuracy of 0.01 g. To evaluate the mineralogical composition and ion concentrations, specimens were completely dried and then sampled in different locations, i.e., the top surface zone and the inner core zone (2.5 cm deep). The extracted small sandstone pieces were ground to a fine powder for X-ray diffraction analysis (D/max2200, Rigaku, Tokyo, Japan). In addition, the powder (0.1 g) was mixed with distilled water (20 mL), after which the mixture was stirred, settled, and filtered prior to the identification of soluble salts using ion chromatography (Dionex Aquion AQ-1200, Thermo Scientific).

4. Results

4.1. Surface Characteristics

Observations using a digital microscope provided details about visual alterations the surfaces of the specimens underwent when in contact with SO₂. As presented in Figure 7, no evident changes were noted in specimen RH40/T25 after 30 cycles, except

that some particles exhibited brown colors. During the weathering process, lusterless powder appeared on top of the original grains, leading to a soiling effect. For specimen RH80/T25, the following features were detected after SO₂ aging: (1) its entire surface became darker compared to the fresh condition and the contamination was particularly obvious on minerals with light colors; and (2) the boundaries between particles were not as clear as before.

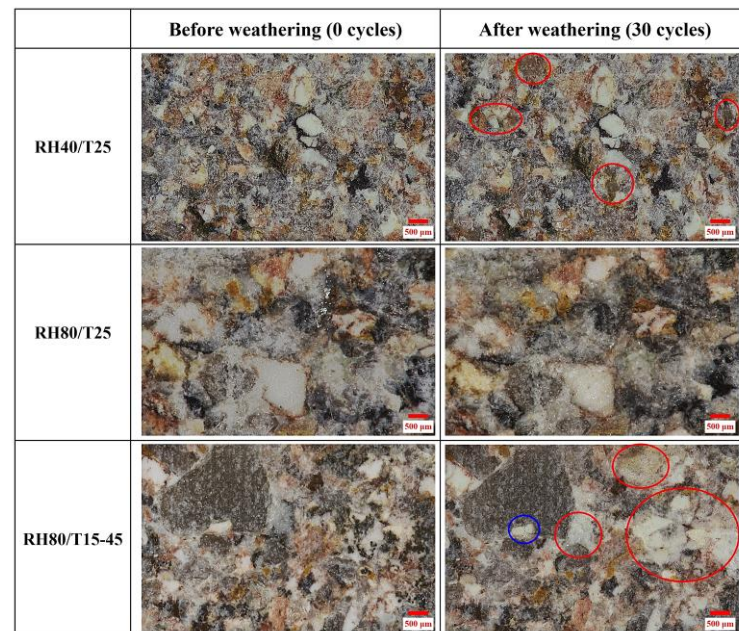


Figure 7. Photographs of surfaces of sandstone specimens before and after weathering tests.

When exposed to the weathering process with temperature fluctuating between 15 and 45 °C, however, the specimen shifted to lighter colors in various locations. Such change was correlated with the detachment of dark minerals and the presence of underlying minerals. In addition, the grain outlines became blurred, accompanied by physical changes of minerals in the form of micro-cracks and fissures (in the blue circle in Figure 7).

4.2. Color Changes

Color changes as a result of aging were characterized based on the CIELab system, in which L^* refers to luminosity or lightness, varying from black with a value of 0 to white with a value of 100, and a^* and b^* are the chromaticity coordinates. More specifically, the coordinates range from $+a^*$ (red, values up to +60) to $-a^*$ (green, values up to -60), and from $+b^*$ (yellow, values up to +60) to $-b^*$ (blue, values up to -60). Color differences are evaluated as follows:

$$\Delta L^* = L_1^* - L_0^*; \Delta a^* = a_1^* - a_0^*; \Delta b^* = b_1^* - b_0^* \quad (1)$$

where L_1^* , a_1^* , and b_1^* are the final values, and L_0^* , a_0^* , and b_0^* are the reference values. Fresh specimens were selected as a reference.

The total color difference (ΔE^*) can be calculated by the following equation:

$$\Delta E^* = \sqrt{\Delta L^{*2} + \Delta a^{*2} + \Delta b^{*2}} \quad (2)$$

It can be seen in Table 5 that for the testing group, the ΔE^* values of specimens after 30 cycles were more than double when the RH in the chamber was increased from 40 to 80%. Specimen RH80/T15-45, which showed an ΔE^* of 1.96, underwent the highest total magnitude of color change. To assess the direction and degree of color modification in detail, the parameters ΔL^* , Δa^* , and Δb^* were also analyzed. Negative values of ΔL^* in

specimens RH40/T25 and RH80/T25 correspond to the blackening of the stone surfaces after weathering, which reflected less light than the original fresh ones. For specimen RH80/T15-45, however, increased lightness was noticed. The results of color measurement are consistent with the observations in Figure 7. Parameters Δa^* and Δb^* indicated changes in the tone of Yungang sandstone. In all three cases, a^* remained almost unchanged, whereas b^* values shifted positively, indicating a slight alteration to yellow hues.

Table 5. Changes in color parameters after artificially accelerated weathering tests.

Specimens		Before Weathering (0 Cycles)			After Weathering (30 Cycles)			
		L^*	a^*	b^*	ΔL^*	Δa^*	Δb^*	ΔE^*
Testing group	RH40/T25	66.04	4.31	5.79	−0.41	0.09	0.47	0.76
	RH80/T25	66.06	4.76	5.61	−1.58	0.13	0.85	1.83
	RH80/T15-45	66.56	4.64	5.83	1.76	0.26	0.73	1.96
Control group	RH40/T25	66.1	4.31	6.21	0.09	0.06	0.07	0.13
	RH80/T25	67.26	5.07	6.77	−0.35	−0.46	0.37	0.71
	RH80/T15-45	66.41	4.61	5.85	0.40	0.35	0.19	0.48

The specific effects of SO₂ gas on the overall color of Yungang sandstone can be revealed by comparing the testing and control groups. As can be seen, the gas led to measurable variations in both ΔL^* and Δb^* after 30 cycles (Table 5). Since the original values of L^* were much higher, the sulfation process was potentially more relevant to shifts in b^* units. Similar results have been reported in previous studies. When exposed to airborne sulfur, the color of the stone was found to change to warmer tonalities (more red and yellow) [9,24,38]. Additionally, the presence of SO₂ also led to an increase in the total color difference of Yungang sandstone. For all test conditions, however, values of ΔE^* were below the color perceptibility threshold, which is generally taken as 3 units in the CIELab space [12,38,39]. This implies that the color change was not visible to the human eye, at least during the investigated time period.

4.3. Weight Changes

Weight change was calculated as the percentage of weight variation with respect to the initial value of the specimen. As presented in Figure 8a, after 30 cycles of exposure in the chamber at 25 °C with 40% RH, the specimens had no or only insignificant changes in weight. The small fluctuations during the cycles were presumably related to variables in the measurement procedure, such as sample handling and balance sensitivity. When RH was increased to 80%, weight gains of 0.27% and 0.94% were observed for specimens in clean and SO₂-polluted atmospheres, respectively (Figure 8b). It can be seen that the weight of specimen RH80/T25 increased continuously throughout the whole weathering process, whereas the weight of the control group stabilized after 10 cycles. The effect of temperature fluctuations on weight change was more pronounced. Regardless of occasional weight loss during the test, in the end, specimen RH80/T15-45 exhibited the highest weight gain (about 1.54%) (Figure 8c). Under the same RH level, the combination of temperature fluctuations and the presence of SO₂ increased the weight gain by a factor of approximately 5.5 compared to that measured under conditions of 25 °C and no SO₂. Weight loss was recorded in the case of temperature fluctuations without SO₂ gas. The weight of the specimens increased at the beginning, followed by a gradual decrease in subsequent cycles.

In fact, weight change is a macroscopic indication of the interaction between the stone and its environment. The fresh Yungang sandstone had been completely oven-dried before the weathering tests. Therefore, once the specimens were placed in the chamber, they began to approach equilibrium with the new environmental conditions. A tendency toward weight increase, particularly at higher RH, was partially attributed to the intake of water vapor, as well as the adsorption of SO₂ gas from the surrounding air. As previously reported, when exposed to a humid acid atmosphere, a series of chemical reactions can be facilitated

in stone, inducing the formation of new compounds. Consequently, the weight of specimens increased to varying degrees with the SO₂ aging cycles [7,19,39,40]. The occasional small weight losses, as shown in Figure 8c, might be explained by the physical decay of the sandstone in the form of granular disintegration or particle detachment. However, this effect was less significant compared to the matter accumulation on specimens over the testing period. Because weight change, a net result of weight gain and loss, is correlated with many different processes, this parameter alone cannot be used to measure the extent of the reaction of the pollutant gases with the stones.

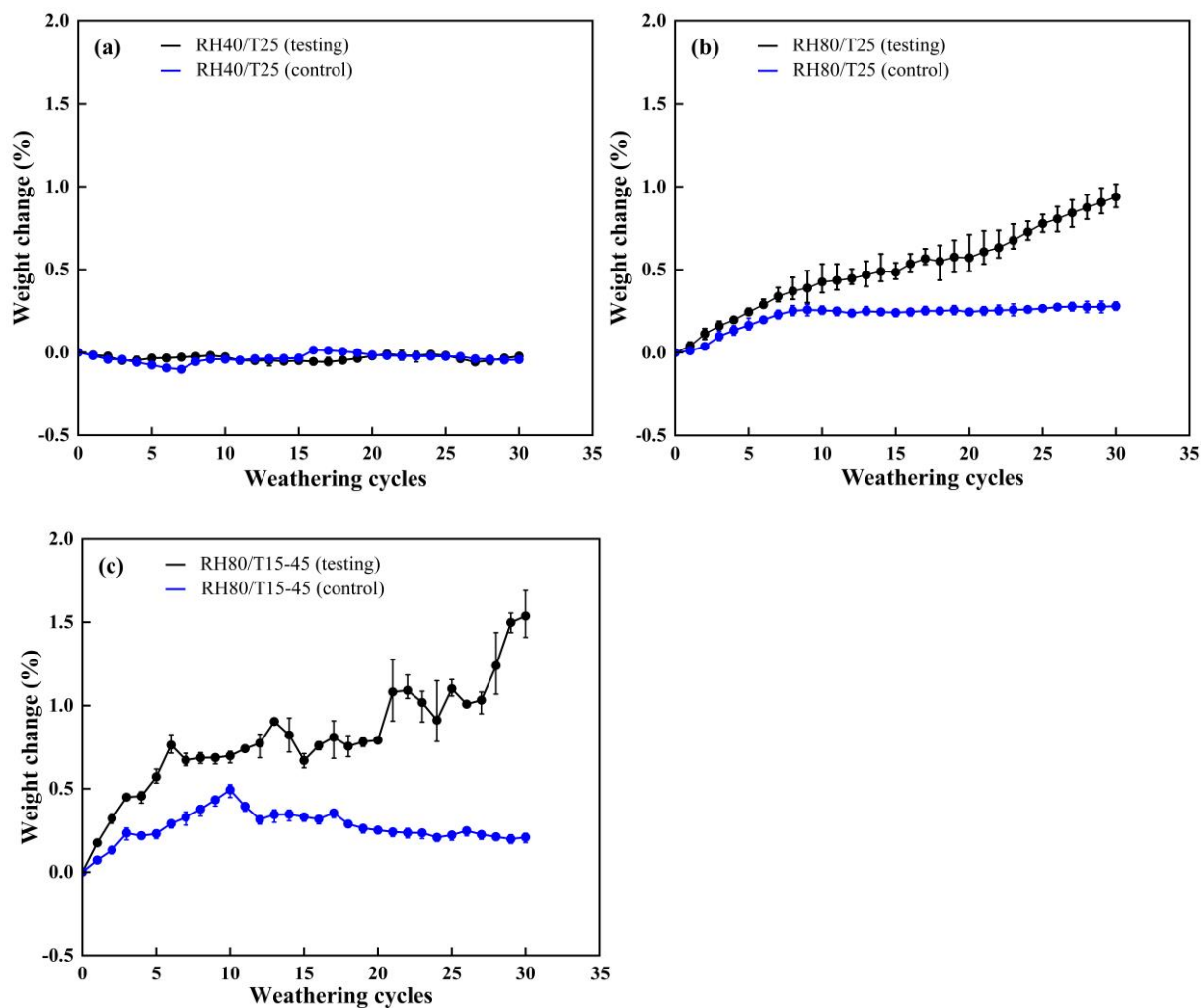


Figure 8. Weight change of sandstone specimens during weathering tests: (a) RH = 40%, T = 25 °C; (b) RH = 80%, T = 25 °C; and (c) RH = 80%, T = 15–45 °C.

4.4. Elemental Composition

The results show that after 30 cycles, loss of Si (1.70%–5.79%) accompanied by a relative increase in Al (0.30%–1.67%) occurred in all specimens in comparison with their fresh status (Table 6). According to [41], decreased silica is one of the principal changes in the chemical weathering of fresh rock, which indicates a great loss of substrate silicates. As silicon loss is often related to total element loss, whereas aluminum is assumed to remain constant during this process, the ratio of silicon to aluminum (Si/Al) can be used to indicate the degree of chemical weathering. It is obvious that in Yungang sandstone, the reduction in the Si/Al ratio was more significant in specimens exposed to higher RH and temperature fluctuations.

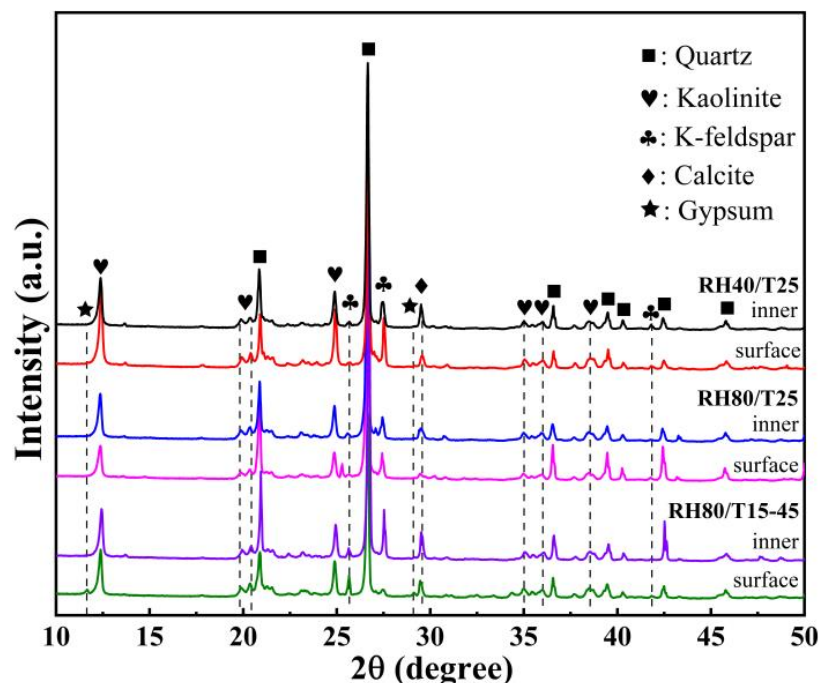
Table 6. Main element composition of specimens (in wt%).

Specimens	Cycles	Si	Al	Ca	Fe	K	Mg	Ti	S
RH40/T25	0	46.14	4.02	1.87	1.02	1.34	2.55	0.10	0.09
	30	44.44	4.32	2.03	1.66	1.10	2.48	0.09	0.49
RH80/T25	0	46.58	4.12	1.44	1.76	1.99	1.99	0.12	0.16
	30	44.73	5.74	2.01	2.33	1.56	2.65	0.11	1.57
RH80/T15-45	0	47.72	4.21	1.68	1.59	1.96	2.25	0.13	0.12
	30	41.93	5.88	1.79	1.43	1.62	1.78	0.06	2.45

As shown in Table 6, enrichment of Ca and S, particularly at the stone surface, was noted in all specimens in the testing group after weathering. Since there was almost no sulfur in the fresh sandstone, the increase in the amount of S revealed a gradual deposition of SO₂ gas on the sandstone during the tests. A similar phenomenon was reported by [42]. Moreover, the content of Fe also increased slightly in the aged specimens, except specimen RH80/T15-45.

4.5. Mineralogical Composition

Figure 9 presents the diffraction patterns of Yungang sandstone after 30 cycles of weathering. The mineral phases in different parts of the specimens in the testing group were analyzed and compared. As can be noticed, the amount of cementing carbonate tended to decrease. The reduction in the main peak of calcite (104), situated at approximately 29.5° 2θ, was more obvious at the surface than in the inner core in all specimens. Due to its instability, calcite exhibited a much higher weathering rate than the other particles in sandstone. According to [5], calcite dissolution is mainly restricted to the finer calcite matrix and cement due to their higher specific surface area.

**Figure 9.** Mineralogical composition of sandstone specimens after weathering tests.

Gypsum is a typical mineral phase that newly forms after the dissolution of calcite in an acid environment containing sulfur. Its most prominent reflection in diffraction patterns appears at 11.5° (020), 20.7° (021), and 29.1° (041). Over the testing period, gypsum was detected only on the surface of specimen RH80/T15-45, which was exposed to 80% RH and temperature fluctuations between 15 and 45 °C. The peaks on the diffraction pattern were

not sharp due to the smaller doses. Considering the detection limit of XRD for salt minerals of around 3%, the absence of gypsum in other specimens can possibly be attributed to the slower reaction rate of SO₂ gas with sandstone under lower RH and constant temperature. In fact, the formation of gypsum is constrained by many factors, including relative humidity and material properties [43].

4.6. Ion Concentrations

The concentrations of the main ions in Yungang sandstone in the testing group, measured using an IC system and with respect to weathering cycles and sampling locations, are presented in Figure 10. For fresh specimens, various types of cations and anions (Na⁺, K⁺, Mg²⁺, Ca²⁺, Cl⁻, SO₄²⁻, and NO₃⁻) were detected, in which Mg²⁺, Ca²⁺, and SO₄²⁻ accounted for over 70% of the total amount of ions. As can be seen, the initial amounts of Mg²⁺, Ca²⁺, and SO₄²⁻ retained in the sandstone were relatively low, varying in ranges of 0.40–2.12, 1.91–3.72, and 3.69–4.46 mg/L, respectively. For each type of ion, concentrations at different locations were similar, indicating a homogeneous distribution in the specimens. The concentrations of all ions exhibited a gradual increase with increasing weathering cycles. Additionally, clear differences were observed between ion concentrations at different depths of the specimen during testing. The variation was more substantial for the surface than for the inner core.

Only traces of Mg²⁺ existed in the fresh Yungang sandstone. In specimens RH40/T25 and RH 80/T25, no noticeable changes in Mg²⁺ concentration occurred either temporally or spatially. In specimen RH80/T15-45, however, the amount of Mg²⁺ retained at the surface and the inner core increased by a factor of about 4 and 2, respectively, after 30 weathering cycles.

Calcium is another important and common cation in stone degradation. After SO₂ aging, the highest Ca²⁺ concentration at the surface was recorded in specimen RH80/T15-45 (37.07 mg/L) and the lowest in specimen RH40/T25 (7.72 mg/L). In the inner core of the specimen, the Ca²⁺ concentration increased from 1.91 to 8.24 mg/L in specimen RH80/T15-45 at the end of testing. In contrast, only a slight increase with time was found in specimens exposed to a constant temperature of 25 °C.

As shown in Figure 10, a drastic increase in the amount of SO₄²⁻ with time, especially at the sandstone surface, indicated obvious deposition of gaseous SO₂. Inward penetration of the gas from the surrounding air and its slow accumulation were also revealed by the presence of more SO₄²⁻ inside the sandstone. For specimens RH80/T25 and RH80/T15-45, the final SO₄²⁻ concentration at the surface reached between 30 and 60 mg/L, which was approximately 8.7 and 15.1 times their respective initial values. In comparison, the final SO₄²⁻ concentration in the inner core of the specimens was lower than 6 mg/L for specimens RH40/T25 and RH80/T25, and nearly 14 mg/L for specimen RH80/T15-45. This indicates that the SO₄²⁻ anion was distributed rather heterogeneously during the weathering process.

It is worth mentioning that the total amounts of Ca²⁺ and Mg²⁺ were stoichiometrically comparable to the amount of SO₄²⁻, suggesting that these cations combine with SO₄²⁻ to form an ion pair. Similar results were presented by previous researchers, who showed that the sulfates of calcium and magnesium were the main secondary salt minerals detected on the weathered sandstone surface at the Yungang Grottoes [44,45]. Other salts, such as sodium and potassium sulfates, may be present in the sandstone material as well. These are aggressive products that induce severe damage by repeated dissolution–crystallization cycles.

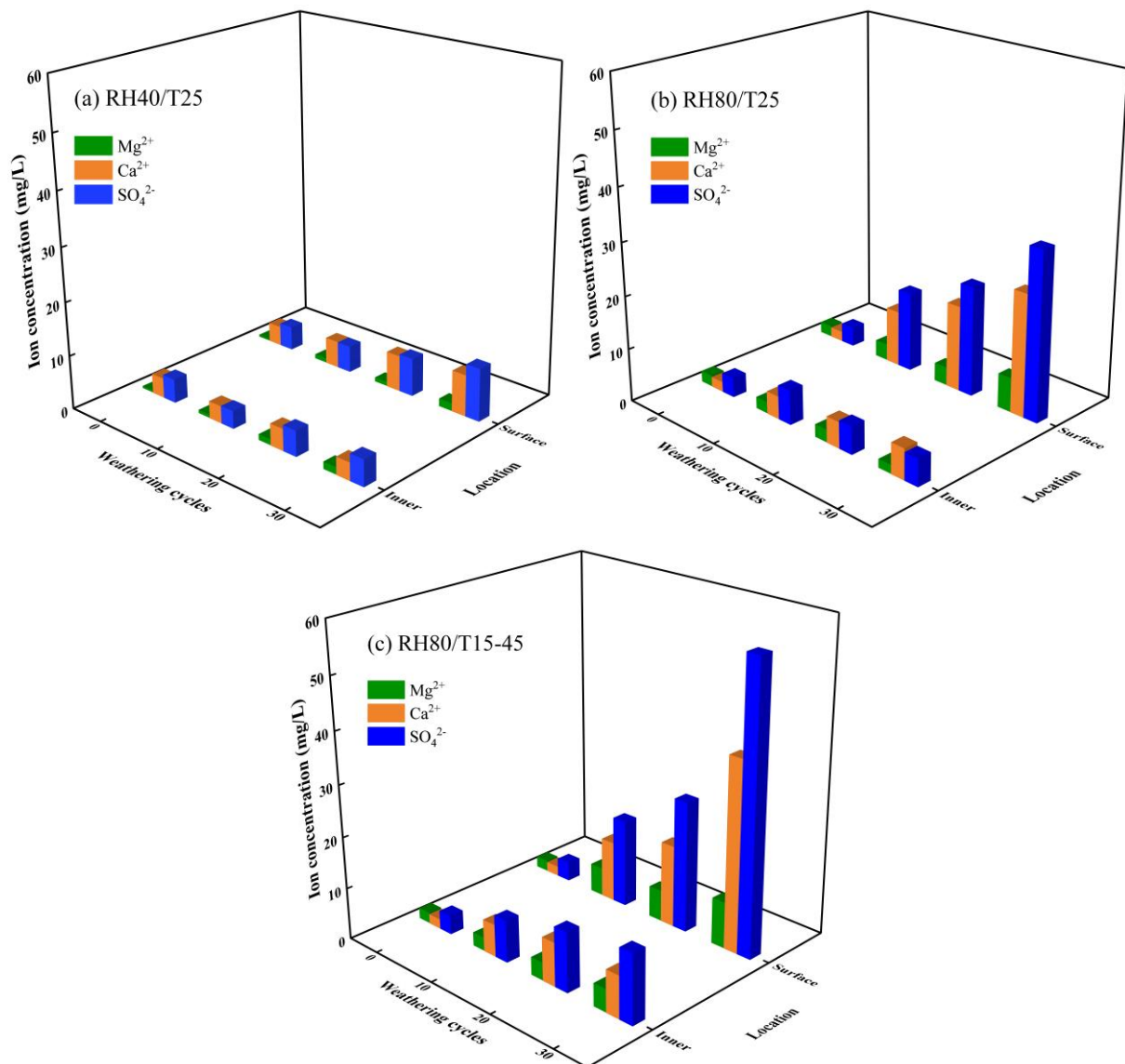


Figure 10. Variation of ion concentrations in sandstone specimens during weathering tests: (a) RH = 40%, T = 25 °C; (b) RH = 80%, T = 25 °C; and (c) RH = 80%, T = 15–45 °C.

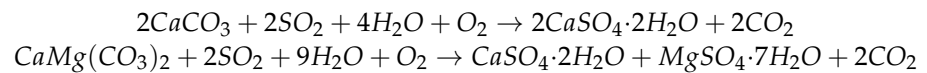
5. Discussion

Although sandstones vary substantially in appearance and durability due to their different geological sources, the dominant mechanisms involved in their deterioration are often similar. Compared to decay related to frost action and salt crystallization, the stone being attacked by acidic gases is a relatively slow process and less easily perceived through observation by the human eye. However, it has been widely recognized that SO₂ from air pollution plays a significant role in stone weathering, promoting both the sulfation of Ca-bearing materials and the kaolinization of feldspar minerals.

5.1. Dissolution of Carbonates

Stone attack by SO₂ is often related to the chemical reactions occurring between this atmospheric gas and the intrinsic calcium-rich minerals contained in stone pores, e.g., calcite, dolomite, plagioclase, and actinolite [10,16,46]. Even if less or no calcium is present in the original stone, it can be derived from an external source, such as an adjacent lime-based joint mortar, other building components made of calcareous stones, and/or aerosol deposition. The end products of a SO₂ attack are calcium sulfate compounds (CaSO₄–H₂O system), which can appear as three distinct minerals: gypsum (dihydrate),

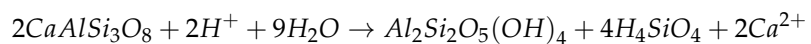
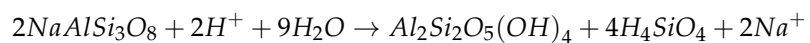
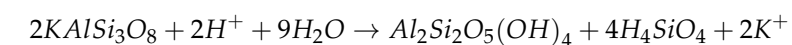
bassanite (hemihydrate), and anhydrite (anhydrous) [40,47]. Gypsum can dehydrate and transform into a lower hydrate; however, these reactions occur in nature on a geological time scale because of the extremely slow kinetics of anhydrite crystallization and the unstable condition of the hemihydrate at temperatures below 42 °C [48]. Therefore, gypsum is the most ubiquitous phase found on historic buildings and heritage sites (Figure 4b). The weathering process of carbonate binders being replaced by gypsum is shown in the following formulas:



The dissolution of carbonate cement around quartz grains might contribute to the formation of larger pores in sandstone. However, the low solubility and mobility of newly formed gypsum favor its accumulation within the pores. The induced pore clogging, especially at the stone surface and subsurface, can prevent water evaporation from the material to some extent. As a result, the sandstone tends to remain damp for longer periods of time. This can cause enhanced migration of soluble salts, biological colonization, and deposition of air pollutants with consequent corrosive reactions. Additionally, the stress generated during gypsum crystallization, rather than the hydration pressure, is also a contributor to the physical deterioration of sandstone. More specifically, when confined in small areas, such as circumgranular pore spaces at the contact between rounded coarse quartz grains or the basal cleavage planes of mica minerals, the growth of gypsum crystals leads to the enlargement of pre-existing micro-cracks and even disruption of the fabric [49]. This phenomenon can have a positive impact on the dissolution of carbonates within deeper zones of stone.

5.2. Hydrolysis of Feldspars

Quartz, one of the predominant constituents of sandstone, is crystalline silica. Its dissolution rate in acids is several orders of magnitude slower than that of carbonate minerals [50]. However, other parent minerals, including feldspars, micas, and chlorites, are not resistant to gaseous SO₂ in the presence of water [15]. They are aluminosilicates, in which silica and alumina are combined with various metal oxides. Once attacked by wet SO₂-polluted air, metal cations such as Ca, K, Na, Mg, and Fe are released from these minerals, transforming into soluble compounds. For example, when feldspar is exposed to weathering by the acidic hydrolysis process, it leaves a secondary clay deposit, which is usually kaolinite [47,49]. The reaction pathway is given by:



During the SO₂ weathering tests described above, certain decomposition of feldspar was indicated in Yungang sandstone specimens by the slight loss of alkali metals, such as potassium (Table 6). Some of the Ca²⁺ ions needed for gypsum crystallization may also derive from this process. Kaolinite is a non-swelling clay and tends not to cause disruptive pressure in the substrate when absorbing water. Nonetheless, the chemical and mineralogical transformation from feldspar to kaolinite could result in various changes in sandstone. In particular, due to the different properties (density, hardness, etc.), and different spaces occupied by the original and new-formed minerals, large amounts of fissures are generated. With increasing kaolinite content, pores generally become larger and more abundant. The presence of secondary kaolinite in a well-cemented quartz sandstone is known to be responsible for a significant reduction in its mechanical strength, as well as its overall durability [33,51,52].

The ions liberated from the original minerals tend to redistribute via transporting, especially toward the stone surface, where they can precipitate and undergo further transformations (Figure 10). Hence, color, one of the most important properties of the stone surface, provides relevant information about the degree of decay during SO₂ exposure. As shown in Table 5, redness and decreased lightness were observed in the weathered specimens. Previous studies indicated that the precipitation and oxidation of metal elements, such as Fe, exposed to an acidic atmosphere may account for such phenomena [11,24,39]. Color changes of stones will show different patterns depending on the material's characteristics, including pore connectivity and initial color, as well as the distribution and oxidation state of Fe. No evident color changes were detected at the surface of the tested Yungang sandstone specimens, possibly because the content of iron was small (less than 2%), the distribution of iron molecules throughout the minerals was not uniform, and the SO₂ aging tests were relatively short.

5.3. Influence of Relative Humidity

Dry deposition refers to the interaction of air pollutants in gaseous form with the stone surface, which can be either wet or dry [7]. When the pollutants are dissolved in atmospheric moisture and present as acid rain, it is known as a wet deposition. The processes of stone deterioration induced by humid SO₂ gas and aqueous SO₂ solution are similar, but with different speeds of interaction [21].

At the site of Yungang Grottoes, many of the sculptures that have survived are situated inside the caves and are therefore sheltered from direct precipitation and runoff. In such a case, the sandstone is reacting permanently with gaseous SO₂ instead of being exposed to acid rain. Water vapor from mist and fog or condensed water can occasionally wet the stone surfaces. Surface moisture not only allows more efficient action of pollutants, including dissolution, dissociation, subsequent transport to places with catalysts, and oxidation, but it also provides a medium for their reaction with minerals, such as calcite [20,53]. In general, a thin moisture film with a thickness of approximately 2 nm appears on the surface of the dry stone at 84% RH [19]. Wiese et al. [50] reported that with increasing RH, both the thickness and coverage of the liquid-like film on mineral grains increase greatly, which might enhance the deposition velocity of SO₂ on stones. As expected, the aeriform mixture of SO₂ gas and water vapor was adsorbed by Yungang sandstone; the higher the ambient RH, the more intensive the SO₂ deposition (Table 6).

Environmental RH also influences gypsum formation. It was reported in [43] that throughout a 4-week exposure test to contaminated atmospheres, no gypsum appeared in calcareous stones with 30% RH, compared to a relatively small amount of gypsum detected at 70% RH. When the RH was increased to 98%, evident gypsum formation occurred in all samples as early as the second week of exposure. For the tested Yungang specimens, a similar trend was observed under higher RH conditions, with higher weight gain and ion concentrations measured (Figures 8 and 10). However, previous researchers noted that this was not the case for stones immersed in liquids or subjected to surface run-off water. Weight loss instead of weight gain was usually noticed because of the intense influence of aqueous acid solutions, such as dissolution and leaching [25,54].

5.4. Influence of Temperature

Microstructural deterioration of sandstone can be induced by temperature variations. There are three underlying mechanisms: thermal stress, thermal fracturing of minerals, and thermal reactions, which dominate in different scenarios [55]. Commonly, thermal stress plays a key role in the lower temperature range, whereas the latter two are important when the temperature is elevated beyond hundreds of degrees centigrade.

As is widely recognized, minerals undergo volumetric changes during heating and cooling. It was observed by environmental scanning electron microscopy (ESEM) that grain boundaries opened and closed when the ambient temperature varied from 293 to 363 K and back to 293 K [56]. Due to the considerably varied anisotropic expansion characteristics of

different minerals, repeated stress is very likely to be induced within individual particles or between adjacent particles during temperature cycles [56,57]. Bulk particles exhibit higher resistance to failure because of their stronger intracrystalline bonds. Consequently, as the thermal stress exceeds the yield stress, cracks and granular decohesion manifest, especially along the particle interfaces and other fabric discontinuities, such as pre-existing micro-fissures. It should also be mentioned that successive changes in the environmental temperature often induce a thermal gradient between the surface of the stone and its interior. In addition, noticeable distinctions between the surface temperatures of different minerals have been measured on the microscopic scale [58]. The more heterogeneous the coexisting mineral phases, the greater the possibility of causing complex stress fields in the material. This will magnify the negative effects of a thermal expansion mismatch on the mechanical properties of stone, enhancing the decay. As shown in Figure 8, all specimens presented a tendency of increasing weight, although it was exceedingly small ($\ll 2\%$ after aging tests). The most likely explanation for the up-and-down changes in the data, especially for specimen RH80/T15-45, is the competition between granular disintegration and precipitation of secondary salt minerals. Obviously, the formation of new products dominates over particle detachment.

High temperature accelerates the rate of chemical reactions as well. The detailed reaction mechanism in an albite-rich rock under acidic solution was studied at the atomic level by performing the ReaxFF reactive molecular dynamics simulation [59]. Changes of H-O bonds in H_2SO_4 and H_2O molecules, and Si-O and Al-O bonds in albite slabs were assessed at 298 and 323 K, respectively. The results showed that the dissociation of H from $\text{H}_2\text{SO}_4/\text{H}_2\text{O}$ molecules accelerated the formation of SO_4^{2-} products. In addition, the breakage of Si-O/Al-O bonds in $\text{SiO}_4/\text{AlO}_4$ tetrahedrons opened a pathway for Na atoms, which became less restricted within the tetrahedron configuration. As the temperature increased, the reaction rate during these processes was promoted. In particular, with increasing available energy and migration channels, more Na atoms could diffuse farther away. According to these findings, a reasonable speculation regarding Yungang sandstone is that under exposure to fluctuating temperatures between 15 and 45 °C, more ions could be released, as indicated by the higher ion concentrations measured by IC (Figure 10).

6. Conclusions

Many grotto heritage sites are suffering degradation related to sulfur dioxide, an acid air pollutant that conservators have been concerned about for decades. In this study, a field investigation was first conducted at the Yungang Grottoes, with analyses of typical weathering features and products on the sandstone surface. Furthermore, a laboratory experiment was carried out on the local sandstone using a specially developed test device. The fresh specimens were subjected to controlled environmental conditions in the weathering chamber, taking into account the influences of gaseous SO_2 , relative humidity, and temperature. During the test, the surface characteristics, color, weight, and chemical and mineralogical compositions of the specimens were measured. The effects of each factor on Yungang sandstone were evaluated to elucidate the deterioration mechanisms. The main conclusions can be drawn as follows:

1. Crust with varying color, morphology, and thickness was one of the typical weathering features observed on the outermost sandstone layer in the caves. The detachment of crusts could have induced further decay, such as contour scaling and granular disintegration. The sulfur content in the weathering products was higher than in the fresh sandstone, suggesting an external source.
2. Under exposure to gaseous SO_2 , the sandstone specimens showed some physical changes. Color changes were found to be mainly due to variations in the ΔL^* and Δb^* parameters. The ΔE^* values were lower than the color perceptibility threshold, suggesting that the changes in color were not visible to the human eye, at least for the period studied. There was also a general trend of weight gain due to the intake of water vapor and SO_2 gas.

3. Chemical and mineralogical changes in sandstone specimens were detected using XRF, XRD, and IC analyses. After weathering, the ratio of silicon to aluminum decreased obviously. A reduction in calcite was observed, especially at the exposed surface, resulting in a gradual increase in Ca^{2+} content. When the cations combined with SO_4^{2-} , a trace of secondary salt minerals, such as gypsum, formed at the end of the test.
4. Sandstone degradation caused by SO_2 deposition is mainly due to the dissolution of carbonates and the hydrolysis of feldspars. Relative humidity and temperature in the environment work together, which can accelerate chemical reactions and thereby enhance the degree of deterioration when increased. Moreover, the granular disintegration of sandstone associated with cyclic temperature fluctuations cannot be ignored.

The complexity of the relationships between stone properties and the environment underlines the importance of studying combinations of decay factors. In most cases, these factors act synergistically and there are many feedback mechanisms in operation. Therefore, it does not make sense to interpret the deterioration processes of sandstone by an isolated, individual factor. In the future, it will be important to carry out outdoor exposure tests in combination with laboratory tests to evaluate the durability of sandstone. More in-depth analyses at different scales (nano-, micro-, meso-, and macro-scales) are also needed to understand the overall context of deterioration.

Author Contributions: Conceptualization, J.H.; Methodology, Y.Z. and C.C.; Formal analysis, C.C.; Investigation, Y.Z. and C.C.; Data curation, H.D., X.G., and J.R.; Writing—original draft, Y.Z.; Writing—review and editing, H.D., J.H., X.G. and J.R.; Visualization, H.D. and Q.L.; Supervision, J.H.; Project administration, J.H.; Funding acquisition, Y.Z. and J.H. All authors have read and agreed to the published version of the manuscript.

Funding: This work was financially supported by the National Key R&D Program of China (No. 2019YFC1520500) and National Natural Science Foundation of China (No. 42007265).

Data Availability Statement: Not applicable.

Acknowledgments: We thank Hongbin Yan and other people from Yungang Academy who provided great help during the fieldwork. We further give our sincere gratitude to Yanmei Tong at Lanzhou University for her assistance with XRD data analysis. The authors are also indebted to Gesa Schwantes for her help with the language editing of the manuscript. All anonymous reviewers are gratefully acknowledged for their careful and insightful reviews.

Conflicts of Interest: The authors declare no conflict of interest.

References

1. Siegesmund, S.; Torok, A.; Hupers, A.; Muller, C.; Klemm, W. Mineralogical, geochemical and microfabric evidences of gypsum crusts: A case study from Budapest. *Environ. Geol.* **2007**, *14*, 103. [[CrossRef](#)]
2. Toniolo, L.; Zerbi, C.M.; Bugini, R. Black layers on historical architecture. *Environ. Sci. Pollut. Res.* **2009**, *16*, 218–226. [[CrossRef](#)] [[PubMed](#)]
3. Torok, A.; Licha, T.; Simon, K.; Siegesmund, S. Urban and rural limestone weathering; the contribution of dust to black crust formation. *Environ. Earth Sci.* **2011**, *63*, 675–693. [[CrossRef](#)]
4. Graue, B.; Siegesmund, S.; Simon, K. The effect of air pollution on stone decay: The decay of the Drachenfels trachyte in industrial, urban and rural environments—a case study of the Cologne, Altenberg and Xanten cathedrals. *Environ. Earth Sci.* **2013**, *69*, 1095–1124. [[CrossRef](#)]
5. De Kock, T.; Van Stappen, J.; Fronteau, G.; Boone, M.; De Boever, W.; Dagrain, F.; Silversmit, G.; Vincze, L.; Cnudde, V. Laminar gypsum crust on lede stone: Microspatial characterization and laboratory acid weathering. *Talanta* **2017**, *162*, 193–202. [[CrossRef](#)]
6. Rovella, N.; Aly, N.; Comite, V.; Randazzo, L.; Fermo, P.; Barca, D.; de Buergo, M.A.; La Russa, M.F. The environmental impact of air pollution on the built heritage of historic Cairo (Egypt). *Sci. Total Environ.* **2021**, *764*, 142905. [[CrossRef](#)]
7. Johnson, J.B.; Haneef, S.J.; Hepburn, B.J.; Hutchinson, A.J.; Thompson, G.E.; Wood, G.C. Laboratory exposure systems to simulate atmospheric degradation of building stone under dry and wet deposition conditions. *Atmos. Environ.* **1990**, *24*, 2585–2595. [[CrossRef](#)]
8. Allen, G.C.; El-Turki, A.; Hallam, K.R.; McLaughlin, D.; Stacey, M. Role of NO_2 and SO_2 in degradation of limestone. *Br. Corros. J.* **2000**, *35*, 35–38. [[CrossRef](#)]

9. Grossi, C.M.; Brimblecomb, P.; Esbert, R.M.; Alonso, F.J. Color changes in architectural limestones from pollution and cleaning. *Color Res. Appl.* **2007**, *32*, 320–331. [[CrossRef](#)]
10. Luque, A.; Martinez de Yuso, M.V.; Cultrone, G.; Sebastian, E. Analysis of the surface of different marbles by X-ray photoelectron spectroscopy (XPS) to evaluate decay by SO₂ attack. *Environ. Earth Sci.* **2013**, *68*, 833–845. [[CrossRef](#)]
11. Eyssautier-Chuine, S.; Marin, B.; Thomachot-Schneider, C.; Fronteau, G.; Schneider, A.; Gibeaux, S.; Vazquez, P. Simulation of acid rain weathering effect on natural and artificial carbonate stones. *Environ. Earth Sci.* **2016**, *75*, 748. [[CrossRef](#)]
12. Cetintas, S.; Akboga, Z. Investigation of resistance to ageing by SO₂ on some building stone. *Constr. Build. Mater.* **2020**, *262*, 120341. [[CrossRef](#)]
13. Giustetto, R.; Pastero, L.; Aquilano, D. Potential effects of the shape of gypsum aggregates on the early sulfation of marble and travertine. *J. Build. Eng.* **2020**, *32*, 101794. [[CrossRef](#)]
14. Germinario, L.; Torok, A. Surface weathering of tuffs: Compositional and microstructural changes in the building stones of the Medieval Castles of Hungary. *Minerals* **2020**, *10*, 376. [[CrossRef](#)]
15. Celik, M.Y.; Ersoy, M.; Sert, M.; Arsoy, Z.; Yesilkaya, L. Investigation of some atmospheric effects in the laboratory tests on deterioration of andesite (Iscehisar-Turkey) used as the building stone of cultural heritages. *Arab. J. Geosci.* **2021**, *14*, 103. [[CrossRef](#)]
16. McKinley, J.M.; Curran, J.M.; Turkington, A.V. Gypsum formation in non-calcareous building sandstone: A case study of Scrabo sandstone. *Earth Surf. Process. Landf.* **2001**, *26*, 869–875. [[CrossRef](#)]
17. Cnudde, V.; Silversmit, G.; Boone, M.; Dewanckele, J.; De Samber, B.; Schoonjans, T.; Van Loo, D.; De Witte, Y.; Elburg, M.; Vincze, L.; et al. Multi-disciplinary characterization of a sandstone surface crust. *Sci. Total Environ.* **2009**, *407*, 5417–5427. [[CrossRef](#)]
18. Marszalek, M.; Alexandrowicz, Z.; Rzepa, G. Composition of weathering crusts on sandstones from natural outcrops and architectonic elements in an urban environment. *Environ. Sci. Pollut. Res.* **2014**, *21*, 14023–14036. [[CrossRef](#)]
19. Haneef, S.J.; Johnson, J.B.; Dickinson, C.; Thompson, G.E.; Wood, G.C. Effect of dry deposition of NO_x and SO₂ gaseous pollutants on the degradation of calcareous building stones. *Atmos. Environ.* **1992**, *26*, 2963–2974. [[CrossRef](#)]
20. Bai, Y.; Thompson, G.E.; Martinez-Ramirez, S.; Brueggerhoff, S. Mineralogical study of salt crusts formed on historic building stones. *Sci. Total Environ.* **2003**, *302*, 247–251. [[CrossRef](#)]
21. Holynska, B.; Gilewicz-Wolter, J.; Ostachowicz, B.; Bielewski, M.; Strel, C.; Wobrauschek, P. Study of the deterioration of sandstone due to acid rain and humid SO₂ gas. *X-Ray Spectrom.* **2004**, *33*, 342–348. [[CrossRef](#)]
22. Behlen, A.; Steiger, M.; Dannecker, W. Deposition of sulfur dioxide to building stones: The influence of the ambient concentration on the deposition velocity. *Environ. Geol.* **2008**, *56*, 595–603. [[CrossRef](#)]
23. Muller, U. The mineralogical composition of sandstone and its effect on sulphur dioxide deposition. *Mater. Constr.* **2008**, *58*, 81–95.
24. Vazquez, P.; Carrizo, L.; Thomachot-Schneider, C.; Gibeaux, S.; Alonso, F.J. Influence of surface finish and composition on the deterioration of building stones exposed to acid atmospheres. *Constr. Build. Mater.* **2016**, *106*, 392–403. [[CrossRef](#)]
25. Franzoni, E.; Sassoni, E. Correlation between microstructural characteristics and weight loss of natural stones exposed to simulated acid rain. *Sci. Total Environ.* **2011**, *412*, 278–285. [[CrossRef](#)] [[PubMed](#)]
26. Ausset, P.; Crovisier, J.L.; Del Monte, M.; Furlan, V.; Girardet, F.; Hammecker, C.; Jeannette, D.; Lefevre, R.A. Experimental study of limestone and sandstone sulphation in polluted realistic conditions: The Lausanne Atmospheric Simulation Chamber (LASC). *Atmos. Environ.* **1996**, *30*, 3197–3207. [[CrossRef](#)]
27. Dewanckele, J.; De Kock, T.; Boone, M.A.; Cnudde, V.; Brabant, L.; Boone, M.N.; Fronteau, G.; Van Hoorebeke, L.; Jacobs, P. 4D imaging and quantification of pore structure modifications inside natural building stones by means of high resolution X-ray CT. *Sci. Total Environ.* **2012**, *416*, 436–448. [[CrossRef](#)]
28. Wang, K.P.; Xu, G.L.; Li, S.T.; Ge, C. Geo-environmental characteristics of weathering deterioration of red sandstone relics: A case study in Tongtianyan Grottoes, Southern China. *Bull. Eng. Geol. Environ.* **2018**, *77*, 1515–1527. [[CrossRef](#)]
29. Zhang, Y.; Zhang, Y.M.; Huang, J.Z. Experimental study on capillary water absorption of sandstones from different grotto heritage sites in China. *Herit. Sci.* **2022**, *10*, 25. [[CrossRef](#)]
30. Zhang, H.; Shi, M.F.; Shen, W.; Li, Z.G.; Zhang, B.J.; Liu, R.Z.; Zhang, R.P. Damage or protection? The role of smoked crust on sandstones from Yungang Grottoes. *J. Archaeol. Sci.* **2013**, *40*, 935–942. [[CrossRef](#)]
31. Qin, Y.; Wang, Y.H.; Li, L.L.; Huang, J.Z. Experimental weathering of weak sandstone without direct water participation by using sandstone from the Yungang Grottoes in Datong, China. *Rock Mech. Rock Eng.* **2016**, *49*, 4473–4478. [[CrossRef](#)]
32. Geng, H.; Zhang, S.J.; Zhi, J.H.; Zhang, R.P.; Ren, J.G.; Ro, C.U. Acid solution decreases the compressional wave velocity of sandstone from the Yungang Grottoes, Datong, China. *Herit. Sci.* **2019**, *7*, 4. [[CrossRef](#)]
33. Zhang, J.K.; Li, Z.; Li, L.; Liu, J.H.; Liu, D.; Shao, M.S. Study on weathering mechanism of sandstone statues in Southwest China: Example from the sandstone of Niche of Sakyamuni Entering Nirvana at Dazu Rock Carvings. *Nat. Hazards* **2021**, *108*, 775–797. [[CrossRef](#)]
34. Salmon, L.G.; Christoforou, C.S.; Cass, G.R. Airborne pollutants in the Buddhist cave temples at the Yungang Grottoes, China. *Environ. Sci. Technol.* **1994**, *28*, 805–811. [[CrossRef](#)]
35. Christoforou, C.S.; Salmon, L.G.; Cass, G.R. Deposition of atmospheric particles within the Buddhist cave temples at Yungang, China. *Atmos Environ.* **1994**, *28*, 2081–2091. [[CrossRef](#)]
36. Christoforou, C.S.; Salmon, L.G.; Cass, G.R. Fate of atmospheric particles within the Buddhist cave temples at Yungang, China. *Environ. Sci. Technol.* **1996**, *30*, 3425–3434. [[CrossRef](#)]

37. Ren, J.G.; Zhang, Z.; Shi, M.F.; Huang, J.Z. An analysis of density variation at Yungang Grottos. *China Cult. Herit. Sci. Res.* **2015**, 85–90. (In Chinese) [[CrossRef](#)]
38. Urosevic, M.; Yebra-Rodriguez, A.; Sebastian-Pardo, E.; Cardell, C. Black soiling of an architectural limestone during two-year term exposure to urban air in the city of Granada (S Spain). *Sci. Total Environ.* **2012**, *441*, 564–575. [[CrossRef](#)]
39. Gibeaux, S.; Thomachot-Schneider, C.; Eyssautier-Chuine, S.; Marin, B.; Vazquez, P. Simulation of acid weathering on natural and artificial building stones according to the current atmospheric SO₂/NO_x rate. *Environ. Earth Sci.* **2018**, *77*, 327. [[CrossRef](#)]
40. Pires, V.; Rosa, L.G.; Amaral, P.M.; Dionisio, A.; Simao, J.A.R. Experimental studies of the effect of SO₂ on the mechanical properties of selected cladding natural stones. *J. Mater. Civ. Eng.* **2022**, *34*, 04022084. [[CrossRef](#)]
41. Ruxton, B.P. Measures of the degree of chemical weathering of rocks. *J. Geol.* **1968**, *76*, 518–527. [[CrossRef](#)]
42. Matsuda, Y.; Mamuro, T. Simultaneous analysis of gaseous and particulate sulfur in the atmosphere by X-ray fluorescence spectrometry. *J. Radioanal. Chem.* **1977**, *36*, 209–219. [[CrossRef](#)]
43. Unterwurzacher, M.; Mirwald, P.W. Initial stages of carbonate weathering: Climate chamber studies under realistic pollution conditions. *Environ. Geol.* **2008**, *56*, 507–519. [[CrossRef](#)]
44. Ma, Z.P.; Huang, J.Z.; Zhang, H. Chemical weathering of carbonate cement in sandstone and the related cultural relic diseases in Yungang Grottoes. *Carsologica Sinica* **2005**, *24*, 71–76. (In Chinese)
45. Liu, R.Z.; Zhang, B.J.; Zhang, H.; Shi, M.F. Deterioration of Yungang Grottoes: Diagnosis and research. *J. Cult. Herit.* **2011**, *12*, 494–499. [[CrossRef](#)]
46. Vidal, F.; Vicente, R.; Silva, J.M. Review of environmental and air pollution impacts on built heritage: 10 questions on corrosion and soiling effects for urban intervention. *J. Cult. Herit.* **2019**, *37*, 273–295. [[CrossRef](#)]
47. Halsey, D.P.; Dews, S.J.; Mitchell, D.J.; Harris, F.C. Real time measurements of sandstone deterioration: A microcatchment study. *Build. Environ.* **1995**, *30*, 411–417. [[CrossRef](#)]
48. Charola, A.E.; Puhlinger, J.; Steiger, M. Gypsum: A review of its role in the deterioration of building materials. *Environ. Geol.* **2007**, *52*, 207–220. [[CrossRef](#)]
49. Schiavon, N. Kaolinisation of granite in an urban environment. *Environ. Geol.* **2007**, *52*, 333–341. [[CrossRef](#)]
50. Wiese, U.; Behlen, A.; Steiger, M. The influence of relative humidity on the SO₂ deposition velocity to building stones: A chamber study at very low SO₂ concentration. *Environ. Earth Sci.* **2013**, *69*, 1125–1134. [[CrossRef](#)]
51. An, W.B.; Wang, L.G.; Chen, H. Mechanical properties of weathered feldspar sandstone after experiencing dry-wet cycles. *Adv. Mater. Sci. Eng.* **2020**, *2020*, 6268945. [[CrossRef](#)]
52. Yao, Q.L.; Yu, L.Q.; Li, X.H.; Yan, K.; Xu, Q.; Wang, W.N.; Tang, C.J. The effect of micro- and meso-scale characteristics on the mechanical properties of coal-bearing sandstone. *Arab. J. Geosci.* **2020**, *13*, 871. [[CrossRef](#)]
53. Al-Hosney, H.A.; Grassian, V.H. Water, sulfur dioxide and nitric acid adsorption on calcium carbonate: A transmission and ATR-FTIR study. *Phys. Chem. Chem. Phys.* **2005**, *7*, 1266–1276. [[CrossRef](#)] [[PubMed](#)]
54. Gibeaux, S.; Vazquez, P.; De Kock, T.; Cnudde, V.; Thomachot-Schneider, C. Weathering assessment under X-ray tomography of building stones exposed to acid atmospheres at current pollution rate. *Constr. Build. Mater.* **2018**, *168*, 187–198. [[CrossRef](#)]
55. Shen, Y.J.; Zhang, Y.L.; Gao, F.; Yang, G.S.; Lai, X.P. Influence of temperature on the microstructure deterioration of sandstone. *Energies* **2018**, *11*, 1753. [[CrossRef](#)]
56. Luque, A.; Leiss, B.; Alvarez-Lloret, P.; Cultrone, G.; Siegesmund, S.; Sebastian, E.; Cardell, C. Potential thermal expansion of calcitic and dolomitic marbles from Andalusia (Spain). *J. Appl. Crystallogr.* **2011**, *44*, 1227–1237. [[CrossRef](#)]
57. Johnson, W.H.; Parsons, W.H. Thermal expansion of concrete aggregate materials. *J. Res. Natl. Bur. Stand.* **1944**, *32*, 101–126. [[CrossRef](#)]
58. Gomez-Heras, M.; Smith, B.J.; Fort, R. Surface temperature differences between minerals in crystalline rocks: Implications for granular disaggregation of granites through thermal fatigue. *Geomorphology* **2006**, *78*, 236–249. [[CrossRef](#)]
59. Wang, J.X. Chemical weathering mechanism of Albite-rich rocks in Grottoes under an acidic environment: An atomistic view from ReaxFF simulation. *Comput. Mater. Sci.* **2022**, *211*, 111498. [[CrossRef](#)]

Disclaimer/Publisher's Note: The statements, opinions and data contained in all publications are solely those of the individual author(s) and contributor(s) and not of MDPI and/or the editor(s). MDPI and/or the editor(s) disclaim responsibility for any injury to people or property resulting from any ideas, methods, instructions or products referred to in the content.